THE JOURNAL OF PHYSICAL CHEMISTRY C
A JOURNAL OF THE AMERICAN CHEMICAL SOCIETY

pubs.acs.org/JPCC

Article

Structure–Property Relationships in Amorphous Thieno[3,2-*b*]thiophene–Diketopyrrolopyrrole–Thiophene-Containing Polymers

Ling Jiang, Jonathan D. Hirst,* and Hainam Do*

Cite This: https://doi.org/10.1021/acs.jpcc.2c01650

Read Online

ACCESS | Metrics & More | Article Recommendations | Supporting Information

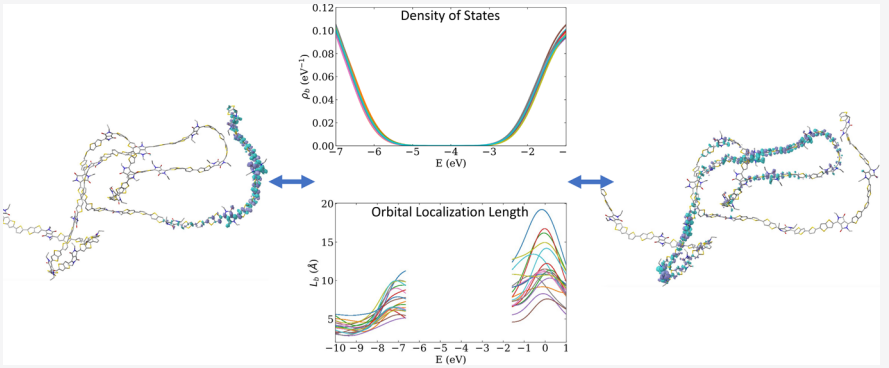

ABSTRACT: We present calculations of electronic structure properties of disordered conducting polymers containing thieno[3,2-*b*]thiophene, diketopyrrolopyrrole, and thiophene. Atomistic force field parameters for the polymer were optimized to minimize the difference between the ab initio and empirical potential energy surfaces and their corresponding first derivatives. These new force fields are employed to propagate the nuclear dynamics, and the equilibrium trajectories are sampled for subsequent electronic structure calculations. We found that the fluctuations of the bulk density of states are negligibly small and do not vary significantly with the length of the backbone and the side-chains. The localization length near the band gap is between 8 and 12 Å, which is about half of the length of the monomer and significantly less than the length of the extended polymer (∼200–400 Å). This indicates that the orbital localization is not affected by the length of the polymer. The inter-chain excitonic couplings are usually smaller than 5 meV, suggesting that the transport mechanism across chains is described by incoherent hopping, and excitons mainly move along the chain. Furthermore, thermal fluctuations cause the evolution of the excitons along the chain. Characterization of the relationships between the geometric disorder of the polymers and the distributions of the lowest excited states reveals that the low-energy excitons tend to localize in regions that are more planar and less folded. However, some excitons are also spread over defects. Thus, our theoretical calculations and the new force fields provide a direct route for characterizing the structure–property relationships and helpful information for constructing more realistic models for the exciton dynamics study of this class of polymeric materials.

INTRODUCTION

Interest in conjugated organic materials, particularly conjugated polymers, is constantly increasing due to the high demand for flexible, light-weight, large-area, easy-to-process, and low-cost electronic applications, such as organic photovoltaics (OPVs),[1−4] the active layer of field-effect transistors (FETs),[5,6] light-emitting diodes (LEDs),[7,8] and bioelectronics.[9,10] Polymeric semiconductors are straightforward to process. The latter's ability to self-assemble, solution processability, deformability, and light weight make them attractive materials for flexible electronic devices. However, these organic semiconductors suffer from low charge mobilities. Conjugated polymers with improved charge mobility would revolutionize the flexible electronics industry. Thus, this research field has seen substantial growth in the last couple of decades[11] with the development of polymer semiconductors with a charge mobility greater than 10 $cm^2 V^{-1} s^{-1}$.[1,2,12]

The π–conjugated backbone in organic semiconducting polymers allows their electronic states to be delocalized across the individual, covalently bonded molecular units. The spatial extent of these electronic states depends strongly on the molecular geometry, and their ability to delocalize across

Received: March 9, 2022
Revised: May 18, 2022

molecular units can be influenced by intermolecular packing. This implies a strong coupling between the electronic and structural dynamics that gives rise to unique and fascinating phenomena.[11] This coupling explains why, over the last two decades, experimental characterizations of the transport properties in organic semiconducting materials have led to a range of seemingly contradictory results.[13] Although qualitative features of charge transport in conjugated polymers have long been established, it is still challenging to quantify the structure−property relationships in these materials.[11,14] By analogy to their inorganic semiconductor counterparts, one might be persuaded that the key ingredient to increasing charge mobilities of organic semiconductors is to improve the local order.[15,16] It turns out that this is only applicable to some but not all classes of conjugated polymers. Examples of high carrier mobility polymers are polythiophenes, e.g., poly(3-hexylthiophene) (P3HT) and poly[2,5-bis(3-alkylthiophene-2-yl)thiono(3,2-*b*)thiophene] (PBTTT), whose mobilities are in the range of 0.1 to 1.0 cm^2s^{-1} V^{-1}.[17] These are highly ordered polymers with relatively large crystalline domains organized into lamellar structures with significant π−stacking.[18] On the other hand, the recent discovery of new high charge mobility amorphous conjugated polymers[19,20] suggests that not all parameters have been taken into account. These contrasting examples indicate the need for robust quantitative models of how (dis)order influences charge mobility in organic semiconducting materials. Therefore, it is crucial to go beyond phenomenological models to capture the interplay between electronic structure properties and the microscopic structure of organic semiconducting polymers.

Investigating the relationship between structure and electronic properties of materials requires constructing atomistic models of the systems of interest and calculating their electronic structure properties. Ab initio molecular dynamics (MD) simulation is the natural choice for this task, as it provides a description at the atomistic scale directly from the first principles of quantum mechanics. However, this technique is limited to only small systems (a few hundred atoms) and is far from tractable for semiconducting polymers comprising tens of thousands of atoms. A remedy to this problem is to employ classical MD simulations to generate an ensemble of equilibrium structures, which are subsequently utilized in large-scale quantum chemistry calculations to obtain the structure−property relationships. However, atomistic modeling of polymers and computing their electronic structure properties are still challenging tasks in their own right from the computational point of view. In addition, one of the main concerns here is the mismatch in the force fields describing the interactions at the classical level and the electronic structure methods employed for subsequent quantum chemistry calculations. Thus, most computational studies in the optoelectronic polymer field have mainly focused on either the structural information using molecular simulations[21−24] or the electronic structure of an isolated polymer chain by quantum chemical calculations.[25−28]

Some attempts have been made to combine MD and electronic structure calculations to characterize the structure−property relationships in conjugated polymers. For example, Simine and Rossky investigated the relationship between the ground-state optical gaps, the properties of the excited states, and the structural features of chromophores of a single molecule poly(3-hexyl)-thiophene (P3HT) using QM/MM simulations.[29] They reported a strong interdependence between the critical aspects of chromophoric disorder and conformational disorder in P3HT. For semi-crystalline polymers, it is possible to investigate the bulk electronic structure property by characterizing one lamella at a time, which drastically reduces the number of atoms in the system. Liu and Troisi used this approach to gain insights into the microscopic origin of the very high charge mobility in PBTTT.[30] Cheung et al.[31,32] examined the connections between charge transfer parameters and the structure of the most studied semiconducting polymer P3HT. The situation is less tractable computationally for amorphous conjugated polymers due to the slow relaxation time (μs timescale) and the size of the systems. Quantum chemical calculations of large models of amorphous polymers are naturally very demanding due to the lack of translational symmetry that would otherwise reduce the size of the problem. Despite these challenges, research along this line has been pursued by several groups. Granadino-Roldán et al.[33] built microscopic models for poly-2,5-bis(phenylethynyl)-1,3,4-thiadiazole (PhEtTh) using MD simulations and then studied the effect of disorder on the electronic couplings, the DOS, and the wave function localization. In the same spirit, Vukmirovic and Wang[34] presented large-scale calculations of the electronic structure of strongly disordered P3HT conjugated polymer models using the density functional theory (DFT)-based charge patching method to construct single-particle Hamiltonian and the overlapping fragments method for the efficient diagonalization of that Hamiltonian. On the other hand, Poelking et al.[35] employed MD and quantum chemical calculations to establish a link between the microscopic ordering and the charge transport parameters for a highly crystalline polymeric organic semiconductor PBTTT. A similar strategy was also employed by Qin and Troisi[36] and Ma et al.[37] to understand the relationships between structure and electronic properties of the amorphous poly(phenylenevinylene) (PPV) derivative MEH-PPV. Despite significant successes, combined morphology−electronic structure study for the excited states of amorphous polymers is still limited by the computational challenges outlined above and by the lack of accurate force fields for conjugated systems.

Diketopyrrolopyrrole (DPP)-based conjugated polymers have emerged as desirable materials for thin-film transistors and solar cell devices. The electron-deficient nature of the DPP core has been exploited to synthesize extremely narrow band gap donor−acceptor-type materials well suited for use in organic photovoltaics with high power conversion efficiencies reported in both small molecules and polymers.[38−40] Furthermore, the planarity of the DPP skeleton and its ability to accept hydrogen bonds result in copolymers that encourage $\pi - \pi$ stacking. Usually, the DPP units are flanked by co-monomers, and variation of the co-monomer yields polymers with attractive properties for both OPV and OFET devices.[41] For instance, copolymerization with thiophene (T), thieno-[3,2-*b*]thiophene (TT) derivatives or benzothiadiazole results in polymers with impressive ambipolar charge-carrier mobilities.[42] Particularly, the TT units extend the polymer coplanarity and promote a more delocalized HOMO distribution along the backbone, enhancing intermolecular charge-carrier hopping.[43] Furthermore, DPP-based semiconducting polymers can achieve a surprisingly high mobility rate without having an overall crystalline structure.[42,44] However, detail of the relationship between the morphology and electronic structure properties of this class of conjugated

https://doi.org/10.1021/acs.jpcc.2c01650
J. Phys. Chem. C XXXX, XXX, XXX−XXX

polymers is still unclear, and a fundamental understanding is necessary for their design and development.

In this paper, we will focus on a recently synthesized TT-flanked DPP and T-containing π-extended conjugated polymers with branched alkyl side-chains[41] poly[[2,5-bis(2-octyldodecyl)-2,3,5,6-tetrahydro-3,6-dioxopyrrolo[3,4-*c*]-pyrrole-1,4-diyl]-*alt*-[[2,2′-(2,5-thiophene)bis-thieno[3,2-*b*]-thiophen]-5,5′-diyl]] (PDPPTT-T-10). The chemical structure of a monomer of this polymer is shown in Figure 1. This

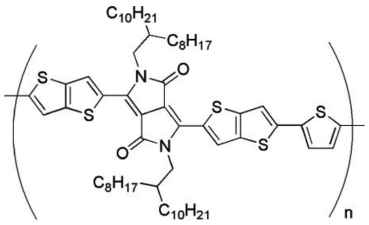

Figure 1. Chemical structure of a monomer of the PDPPTT-T-10 polymer.

polymer has attracted much attention due to its excellent hole mobility and high power conversion efficiency (PCE) when integrated into heterojunction-type polymer solar cells.[41] We first construct a reliable force field and then use MD simulations to generate several large-scale amorphous polymeric models of PDPPTT-T-10. Subsequently, quantum chemical calculations are employed to study the electronic structure properties of these models. Our goal is to provide insights into the electronic excited states of the polymer chains and their connections to the dynamic disorder of the nuclei.

METHODS

Force Field Development. In MD simulation, it is vital that the force fields used to describe the nuclear dynamics are accurate enough to capture the actual molecular motion of the system. A challenge one often has to confront here is the mismatch in the description of the interactions at the classical level and the electronic structure methods employed for subsequent quantum chemistry calculations. To overcome this, we employ our extension[24] of the adaptive force-matching technique[45] to parameterize the force fields for the studied conjugated polymers. The idea behind the procedure is to find a set of parameters that minimizes the differences between the classical and the ab initio forces. Thus, by design, the force fields used to propagate the nuclear dynamics are comparable to those targeted ab initio methods used in the subsequent electronic structure calculations. The procedure for parameterizing the force field is included in the SI.

Classical MD Simulations of the Conjugated Polymers. MD simulations are performed using our new force fields within the NAMD package[46] to generate models of the PDPPTT-T-10 bulk polymer. Systems of 20 chains of 20 monomers/chain (20ch_20mers) and 20 chains of 40 monomers/chain (20ch_40mers) are characterized. The initial structure is prepared with an arbitrary low-density arrangement for each system. Polymer chains are added into the simulation box by growing segment by segment using the configurational bias Monte Carlo technique.[47] The result of this procedure is that low-energy sites are preferred over high-energy sites. Thus, disordered bulk systems containing chains in realistic equilibrium conformations are created. Details of the simulations are outlined in the SI.

The variation of the density in the NPT ensemble simulations with respect to time is shown in Figure 2 for

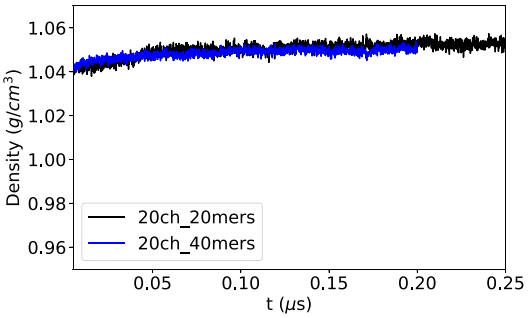

Figure 2. Time evolution of the densities of the 20ch_20mers (black line) and the 20ch_40mers (blue line) systems during the NPT ensemble equilibration.

both the (20ch_20mers) and (20ch_40mers) models. After about 0.2 μs, both systems converge to the same density of about 1.05 g/cm^3. This value is close to what was obtained for a similar conjugated polymer in our previous work[24] and falls within the density range of amorphous conjugated polymers.[48,49] The same final density is also found for other runs starting with different initial configurations. This suggests that reliable models for the amorphous phase of PDPPTT-T-10 can be generated from our procedure.

Quantum Chemical Calculations. To make the quantum chemical calculations tractable for the polymer models, the long-chain alkyl side group is replaced by an ethyl group, which speeds up the excited state calculations without altering the nature of the frontier orbitals. Point charges are added in the position of the surrounding atoms on other polymers to represent the electrostatic environment around the chain of interest. In addition, since the excitonic couplings between polymer chains are insignificant and could be neglected in amorphous conjugated polymers,[36,37] the electronic structure properties are computed separately for each chain. This assumption is verified later in the Results and Discussion section.

We employ time-dependent density functional theory (TDDFT) to characterize the electronic excitation of the amorphous polymer models. The long-range corrected ωB97XD[50] functional in conjunction with the 3-21G* or 6-31G* basis set is utilized to compute the lowest five singlet states. The choice of the functional is based on its ability to capture both short- and long-range interactions and to describe charge transfer states accurately. The effects of the size of the basis set and the number of electronic states included in the calculations are discussed in the Results and Discussion section. Results obtained using other popular functionals, including B3LYP,[51] CAM-B3LYP,[52] and M06-2X[53] are also reported and compared with the results obtained from ωB97XD. To investigate the excited state properties of the polymer, we analyze the DOS, the absorption spectra, the localization length of the one-electron state,[36] the natural transition orbitals, and the electron−hole (e-h) distributions. All quantum chemical calculations are performed with the Gaussian16 program package,[54] while the electronic structure−property analysis is done using the Multiwfn codes.[55]

The inter-chain excitonic coupling $J_{mn}^{\alpha\beta}$ between the exciton α in chain m and the exciton β in chain n is computed using the

https://doi.org/10.1021/acs.jpcc.2c01650
J. Phys. Chem. C XXXX, XXX, XXX−XXX

distributed monopole approximation expressed as a Coulomb interaction term

$$J_{mn}^{\alpha\beta} = \frac{1}{4\pi\epsilon_0\epsilon_r}\sum_{i\in m}\sum_{j\in n}\frac{q_i^t(\alpha)q_j^t(\beta)}{|\mathbf{r}_i - \mathbf{r}_j|} \tag{1}$$

where ϵ_0 is the vacuum permittivity, ϵ_r is the relative permittivity of the polymer, $\mathbf{r}_i$ is the position of atom i, and $q_i^t(\alpha)$ is the atomic transition charge at atom i between the ground state and the α excited state of chain m.

The DOS per chain per monomer $\rho_{c,i}(E)$ is defined as $\rho_{c,i}(E) = \sum_m \delta(E - E_i^m)/M$, where E_i^m is the energy of the molecular orbital m of chain i and M is the total number of monomers per chain.[36] Since the inter-chain excitonic coupling is negligible (see the Results and Discussion section), the bulk DOS of the whole system is calculated by summing the contribution of individual chains as $\rho_b(E) = \sum_i \rho_{c,i}(E)/N_c$, where N_c is the total number of chains. Similarly, the absorption intensity of the ith chain is defined as $I_i(E) = \sum_n f_{0\to n}(i)\delta(E - E_i(n))$, where $f_{0\to n(i)}$ is the oscillator strength for the transition between the ground and the nth excited state of chain i and $E_i(n)$ is the corresponding transition energy. The bulk absorption intensity of the polymer is then calculated as $I_b(E) = \sum_i^N I_i(E)/N_c$.

We define the localization length for molecular orbital m as[36]

$$L^m = 2\left(\sum_{k=1}^{M}|\mathbf{r}_k - \mathbf{R}^m|^2 P_k^m\right)^{1/2} \tag{2}$$

where r_k is the position of the center of mass of monomer k and $R^m = \sum_{k=1}^{M} r_k P_k^m$ is the centroid of the molecular orbital m. P_k^m is the weight of the molecular orbital m on a given monomer k. More information on the definition and calculation of P_k^m can be found from the SI. Then, an energy-dependent localization length for chain i is defined as

$$L_{c,i}(E) = \frac{\sum_m L^m \delta(E - E_i^m)}{\sum_m \delta(E - E_i^m)} \tag{3}$$

and finally the bulk localization length of the system is calculated as

$$L_b(E) = \sum_{i=1}^{N} L_{c,i}(E)/N_c \tag{4}$$

For numerical calculations, $\delta(E - E_i^m)$ and $\delta(E - E_i(n))$ are approximated with a normalized Gaussian of standard deviation $\sigma = 0.5$ eV.

A single-electron excitation is generally described as the process of an electron leaving the hole. The combination of the hole and the electron (if treated as quasi-particles) is often termed an exciton. For example, in the case of a HOMO → LUMO transition, the hole and the electron could be represented by the HOMO and the LUMO, respectively. In practice, the single molecular orbital pair representation (in the canonical form) of an excitation usually is not adequate. The excitation must be treated as a transition involving multiple molecular orbital pairs with corresponding weights. This poses a challenge in representing the hole and electron when there is no dominant molecular orbital pair in a transition. In this instance, canonical molecular orbitals are usually transformed to natural transition orbitals. A more robust approach is to define the hole and the electron in terms of their densities ρ^{hole} and ρ^{elec} (if the phase information is not required) as[55,56]

$$\begin{aligned}\rho^{\text{hole}}(\mathbf{r}) &= \rho_{\text{loc}}^{\text{hole}}(\mathbf{r}) + \rho_{\text{cross}}^{\text{hole}}(\mathbf{r})\\ &= \sum_i^{\text{occ}}\sum_a^{\text{vir}}(w_i^a)^2\varphi_i(\mathbf{r})\varphi_i(\mathbf{r})\\ &\quad + \sum_i^{\text{occ}}\sum_{j\neq i}^{\text{occ}}\sum_a^{\text{vir}} w_i^a w_j^a \varphi_i(\mathbf{r})\varphi_j(\mathbf{r})\end{aligned} \tag{5}$$

$$\begin{aligned}\rho^{\text{elec}}(\mathbf{r}) &= \rho_{\text{loc}}^{\text{elec}}(\mathbf{r}) + \rho_{\text{cross}}^{\text{elec}}(\mathbf{r})\\ &= \sum_i^{\text{occ}}\sum_a^{\text{vir}}(w_i^a)^2\varphi_a(\mathbf{r})\varphi_a(\mathbf{r})\\ &\quad + \sum_i^{\text{occ}}\sum_a^{\text{vir}}\sum_{b\neq a}^{\text{vir}} w_i^a w_i^b \varphi_a(\mathbf{r})\varphi_b(\mathbf{r})\end{aligned} \tag{6}$$

where i and a run over all occupied and virtual molecular orbitals, "loc" and "cross" stand for the contributions of the local and cross terms to the hole and electron distribution, w_i^a is the configuration coefficient (weight) of the corresponding $i \to a$ orbital pair transition, and φ denotes the molecular orbital wavefunction. Since the molecular orbitals are orthonormal and the sum of the square of all configuration coefficients is one (i.e., $\sum_i^{\text{occ}}\sum_a^{\text{vir}}(w_i^a)^2 = 1$), it follows that the integration of the densities of the "hole" and the "electron" must also converge to one (i.e., $\int\rho^{\text{hole}}(\mathbf{r})d\mathbf{r} = 1$ and $\int\rho^{\text{elec}}(\mathbf{r})d\mathbf{r} = 1$), indicating an electron is excited. The contribution of an atom A to, for example, the hole, is evaluated using the Hirshfeld partition approach as $\int\rho^{\text{hole}}(fr)w_A(\mathbf{r})d\mathbf{r}$. Finally, the weight of the hole/electron on a given monomer is simply the sum of the contributions of the atoms that belong to the monomer.

To characterize the electronic excitation of the polymer, we analyze the electron−hole (e-h) distributions and the transition density matrix for the lowest five singlet states of single chains. The weight of the transition density from the ground state S_0 to an excited state S_n of monomer k, $P_k^{S_0\to S_n}$, is defined and explained in the SI. The delocalization extent of various electronic excitations is quantified by the participation index (PI), which is the count of the number of monomers that contribute more than 5% to those transitions. The exciton binding energy, which is the negative value of the Coulomb attractive energy between the hole and the electron, can be employed to investigate their degree of separation. This quantity is computed using the Coulomb formula as $E_{\text{coul}} = \int\int\rho^{\text{hole}}(\mathbf{r}_1)\rho^{\text{elec}}(\mathbf{r}_2)/|\mathbf{r}_1 - \mathbf{r}_2|d\mathbf{r}_1 d\mathbf{r}_2$. The extent of the spatial distribution of the hole and the electron is characterized by the root mean squared deviation (RMSD). The x component of the RMSD of the hole can be expressed, for example, as σ_{hole}, $x = \sqrt{\int(x - X_{\text{hole}})^2\rho^{\text{hole}}(\mathbf{r})d\mathbf{r}}$. Then, the differences between the RMSD of the electron and hole, $\Delta\sigma_\lambda$, can be obtained via $\Delta\sigma_\lambda = \sigma_{\text{elec},\lambda} - \sigma_{\text{hole},\lambda}$, where $\lambda = \{x, y, z\}$. Subsequently, the total difference is measured via the $\Delta\sigma$ index, which is $|\boldsymbol{\sigma}_{\text{elec}}| - |\boldsymbol{\sigma}_{\text{hole}}|$. The H-index, given by $(|\boldsymbol{\sigma}_{\text{elec}}| + |\boldsymbol{\sigma}_{\text{hole}}|)/2$, gives the average degree of the spatial extent of the hole and the electron distribution in space. In addition, we also use the Δr- index,[57] which can be interpreted in terms of the hole−electron distance, to characterize the excited states of the polymer.

https://doi.org/10.1021/acs.jpcc.2c01650
J. Phys. Chem. C XXXX, XXX, XXX−XXX

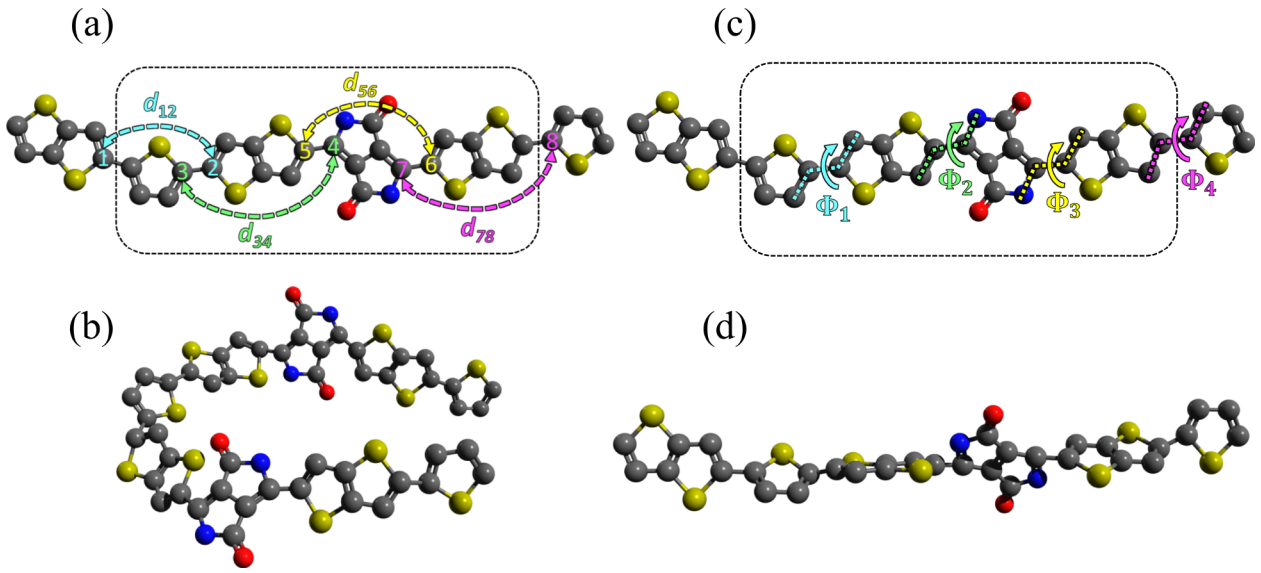

Figure 3. Definition and illustration of chain folding and chain nonplanarity within a PDPPTT-T-10 single chain. Only the backbone atoms are shown for clarity. Atoms within the dotted frames in (a) and (c) belong to a monomer unit. In panel (a), d_{12}, d_{34}, d_{56}, and d_{78} are distances between two carbon atoms in alternating aromatic rings separated by another ring. The average of these distances (within a monomer) gives the folding degree per monomer. In panel (c), Φ_1, Φ_2, Φ_3, and Φ_4 are dihedral angles that account for the nonplanarity within a monomer. Panels (b) and (d) depict the folding and nonplanarity in the polymer, respectively.

Folding and Nonplanarity Parameters. We use the folding and nonplanarity parameters[36] to characterize the relationships between the chain conformation and electronic structure properties in the PDPPTT-T-10 polymer. The folding degree in a PDPPTT-T-10 chain is related to d_{12}, d_{34}, d_{56}, and d_{78} (Figure 3a), which are distances between two carbon atoms in alternating aromatic rings separated by another ring (within a monomer). The deviation of these distances from their equilibrium (perfect planar structure) values can represent the degree of chain folding at monomer k. Thus, we define the average folding degree of monomer k, $\bar{\Delta}^{d}_{k}$, as

$$\bar{\Delta}^{d}_{k} = \sum_{i=1}^{4} (d_i - d_i^e)/4 \tag{7}$$

where d_i are d_{12}, d_{34}, d_{56} and d_{78}, and d_i^e are their corresponding equilibrium values in the perfect planar geometry. Similarly, we define a torsion angle displacement from planarity as $\Delta^{\Phi}_{k} = \min\{|\Phi|, 180 - |\Phi|\}$, where Φ denotes the four dihedral angles (Φ_1, Φ_2, Φ_3, and Φ_4) that mainly account for the nonplanarity within a monomer unit (Figure 3c). The nonplanarity degree of monomer k, $\bar{\Delta}^{\Phi}_{k}$, is then defined as

$$\bar{\Delta}^{\Phi}_{k} = \sum_{j=1}^{4} \Delta^{\Phi_j}_{k}/4 \tag{8}$$

RESULTS AND DISCUSSION

Effects of Basis Set Sizes, Functionals, Side-Chain, and Chain Length. To assess the choice of DFT functionals on the computed electronic excitations of the amorphous PDPPTT-T-10 polymer, we use 20 polymer chains in the 20ch_20mers system at 200 ns (in the NVT ensemble) to make preliminary comparisons. Figure 4a shows the computed absorption spectra for the amorphous polymer using TDDFT with the hybrid functional B3LYP, the hybrid meta functional M06-2X, and the long-range corrected functionals CAM-B3LYP and ωB97XD. For comparison, the same set of spectra is also calculated for an order π-stacked assembly in which

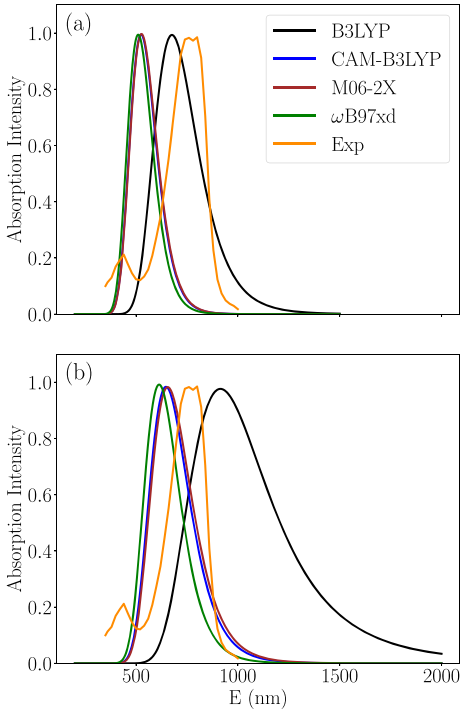

Figure 4. Absorption spectra for a disorder (a) and an order (b) 20ch_20mers system computed using the B3LYP (black line), CAM-B3LYP (blue line), M06-2X (red line), and ωB97XD (green line) functionals. All systems use the 3-21G* basis set. Five lowest singlet excitations are included in the absorption spectra calculation of each chain. The disorder system is taken from the last snapshot (t = 200 ns) in the NVT ensemble run. The order system is taken from a π-stacked assembly in which planar chains align closely in a parallel. Experimentally measured spectra for thin film polymer[43] are also included (orange line).

https://doi.org/10.1021/acs.jpcc.2c01650
J. Phys. Chem. C XXXX, XXX, XXX−XXX

planar chains align closely in a parallel (4b). Out of all functionals, B3LYP noticeably underestimates the excitation energy. This is a limitation of the standard hybrid exchange-correlation functionals, which often fail to describe charge-transfer states and $\pi \rightarrow \pi^*$ transitions in extended conjugated systems. They do not exhibit the correct $1/r$ asymptotic behavior,[58] which is crucial for accurately describing the Rydberg excitation energies, oscillator strengths, and charge-transfer excitation energies.[59] Conventional DFT functionals (including the most popular DFT functional in quantum chemistry B3LYP) calculations often underestimate these properties.[59] A remedy to this is employing the long-range corrected exchange-correlation density functionals such as ωB97XD and CAM-B3LYP. The global hybrid M06-2X functional with double the amount of nonlocal exchange has also been shown to improve the description of valence excitations in π-conjugated systems.[53] Figure 4 indicates that the differences in the computed absorption spectra using the three improved functionals (CAM-B3LYP, ωB97XD, and M06-2X) are insignificant.

B3LYP reproduces experimental spectra quite well for amorphous but not for ordered structures. In addition, it cannot capture the long-range behavior, hence failing to describe satisfactorily excited state properties in molecular aggregates.[60] Therefore, we still employ the ωB97XD functional for all other excited state calculations because this functional has the correct $1/r$ asymptotic behavior. While the solvent effects may somewhat contribute to the differences between the computed and experimental spectra, they cannot solely account for this discrepancy, which is more related to the order of the polymer film, as indicated in Figure 4. The calculated spectra of the ordered structures agree better with the experimental spectra, especially those calculated using long-range functionals. In addition, in this case, DFT could reasonably predict the shape of the experimental spectrum. However, large molecular systems require a substantial number of excited states to generate a detailed spectrum. The shoulder at around 400 nm in the experimental absorption spectrum can also be captured by DFT, given that the number of excited states is adequately included in the calculation of the simulated spectra. To demonstrate this, we computed the absorption spectra for an ordered system with chains containing four monomers. This system requires more than 100 excited states to capture the shape of the experimental spectra (Figure S1). For the 20ch_20merssystem, the required number of states would be much more, making it prohibitively difficult to achieve with the current computing technology.

We analyze the snapshots of the amorphous polymers at 200 ns (in the NVT ensemble) to characterize the effects of the size of the basis sets, side-chain, and the chain length on the computed excited state properties. Figure 5a shows that the difference in the computed DOS is almost negligible between the use of the 3-21G* and 6-31G* basis sets. Likewise, Figure 5b illustrates that the alkyl side-chains do not significantly alter the bulk electronic structure properties of the polymer. The use of an ethyl group (in place of the long-chain alkyl side-chain) is adequate for calculating the excited state properties. Furthermore, the bulk DOS computed for the 20mers system is more or less the same as that computed for the 40mers (Figure 5c), suggesting that a chain of 20 monomers is sufficient to represent the bulk amorphous PDPPTT-T-10 polymeric system. Similar trends are also observed for the computed bulk molecular orbital localization lengths and

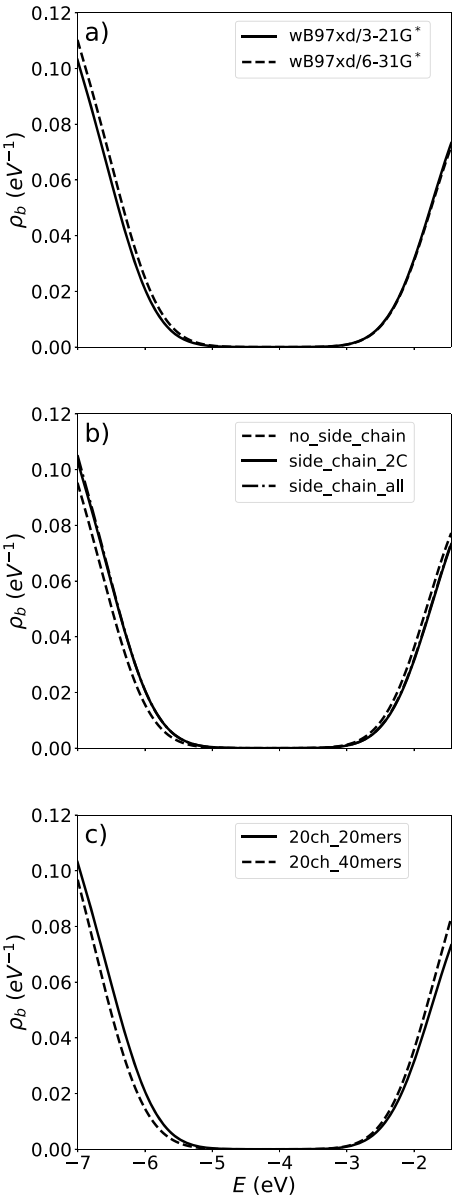

Figure 5. Comparison of the bulk density of states of the PDPPTT-T-10 amorphous polymer using (a) different basis sets, (b) different side-chains, and (c) different chain lengths. The 20ch_20mers system is used to obtain results shown in (a) and (b). Data in (b) and (c) are computed at the ωB97XD/3-21G* level of theory.

absorption spectra of the amorphous polymers. Therefore, to save computational cost, we mainly focus on analyzing the properties of the 20ch_20mers polymeric system using the smaller basis set (3-21G*) and the reduced side-chain (ethyl group).

Figure 6 shows the averaged (over 10 snapshots) bulk DOS and bulk orbital localization length (OLL_b) of the amorphous PDPPTT-T-10 polymer. The bottom panel (Figure 6b) indicates that the states near the gap tend to be localized. The localization length in this region is about 8 Å, which is significantly smaller than the length of the extended polymer (~100 Å) and the average radius of gyration of the system (~40 Å). This is also an indication that the size of the studied polymer (20 to 40 monomers) is adequate and should not influence the orbital localization. The convergence of the electronic properties observed here is based on the assumption

https://doi.org/10.1021/acs.jpcc.2c01650
J. Phys. Chem. C XXXX, XXX, XXX−XXX

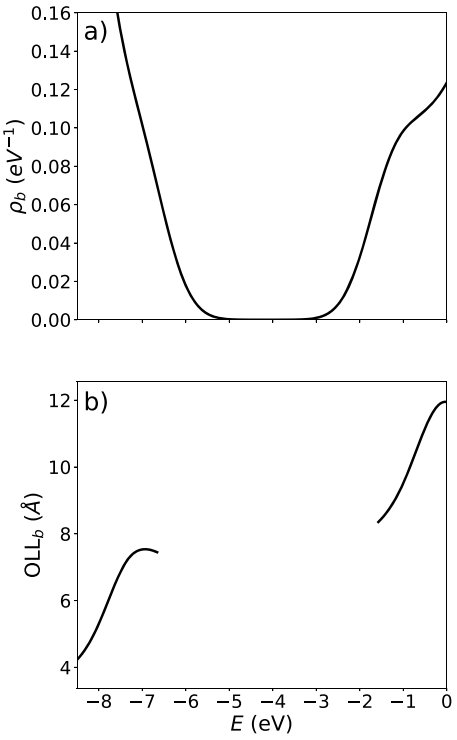

Figure 6. Bulk density of states (a) and bulk orbital localization length (b) for the 20ch_20mers system averaged over 10 snapshots using the trajectories taken from the 200 ns NVT equilibrium run. Each snapshot is separated by 20 ns. Results are obtained using TDDFT at the ωB97XD/3-21G* level of theory.

that the change of the molecular weight does not significantly alter the polymer morphology. For higher molecular weight systems, chain entanglement and aggregation may become important, and in such instances, it is necessary also to correlate these morphological changes to the electronic structure properties.

Interchain Excitonic Coupling. To demonstrate that it is reasonable to consider only the electronic structure of individual chains (as mentioned in the Methods Section), we characterize the interchain excitonic couplings in the amorphous PDPPTT-T-10 polymers. For each chain pair, we evaluate a total of nine excitonic couplings between the three lowest excited states of each chain. Figure 7 shows the histogram distribution of the absolute values of the interchain couplings $|J_{mn}^{\alpha\beta}|$ between the exciton α in chain m and the exciton β in chain n. Figure 7 shows that most couplings are less than 10 meV (more than 95%). There are a few cases where the couplings approach 25 meV, but their probabilities are negligibly small, and values beyond 25 meV are rarely observed. Furthermore, about 90% of the coupling values are less than 5 meV, which indicates that our excited state calculations based on the individual chain calculations are justifiable due to the low probability of exciton hopping between chains. A similar phenomenon is also observed for amorphous MEH-PPV polymers,[37] which implies that this could be a general feature, thus suggesting routes to construct a model for exciton transport in amorphous conjugated polymers.

Charge Transfer Character and Electron−Hole Distribution. To characterize the nature of the electronic transitions of the bulk PDPPTT-T-10 conjugated polymer, we analyze the e-h distributions and the transition densities for

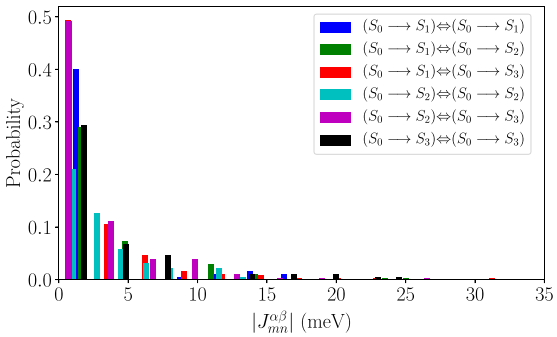

Figure 7. Distribution of the interchain excitonic couplings $(S_0 \rightarrow S_1) \Leftrightarrow (S_0 \rightarrow S_1)$ (blue), $(S_0 \rightarrow S_1) \Leftrightarrow (S_0 \rightarrow S_2)$ (green), $(S_0 \rightarrow S_1) \Leftrightarrow (S_0 \rightarrow S_3)$ (red), $(S_0 \rightarrow S_2) \Leftrightarrow (S_0 \rightarrow S_2)$ (cyan), $(S_0 \rightarrow S_2) \Leftrightarrow (S_0 \rightarrow S_3)$ (magenta), and $(S_0 \rightarrow S_3) \Leftrightarrow (S_0 \rightarrow S_3)$ (black) for 20ch_20mers chain pairs from an equilibrium snapshot (at 200 ns in the NVT ensemble simulation).

the lowest five singlet excitations of the 20ch_20mers from a snapshot taken at 200 ns from the production dynamics. We compute several key metrics (descriptors) of these excited states, including the participation index, the average degree of the spatial extent of the e-h distribution (H-index), the exciton binding energy (E_{coul}) and the average e-h distance upon excitation (Δ_r-index). The values of these descriptors are given in Tables S1−S20, and histograms are shown in Figure S1. The averages of the descriptors are summarized in Table 1. We can

Table 1. Computed Average Electronic Excitation Indices for the Five Lowest Singlet Excited States of the 20ch_20mers System at 200 ns in the NVT Ensemble

transition	$\langle PI \rangle$	$\langle H \rangle$ (Å)	$\langle E_{coul} \rangle$ (eV)	$\langle \Delta r \rangle$ (Å)
$S_0 \rightarrow S_1$	2.35	10.35	1.58	9.54
$S_0 \rightarrow S_2$	2.95	11.71	1.45	10.21
$S_0 \rightarrow S_3$	3.35	14.62	1.08	12.19
$S_0 \rightarrow S_4$	3.25	14.53	1.09	11.05
$S_0 \rightarrow S_5$	3.85	15.81	0.92	10.79

observe from this table that the lowest excited state S_1 has the smallest PI values (just over 2), indicating that, on average, this transition is mainly localized on two monomers. The second, third, and fourth excited states have similar PI values and are more delocalized with PI values around three repeating units. The fifth transition has the highest PI value. This excited state, on average, is delocalized over about four monomers. The exciton energies also confirm this trend; the $S_0 \rightarrow S_1$ transition has the highest binding energy, while $S_0 \rightarrow S_5$ has the lowest. Similarly, we can also observe the low values in the spatial extent of the excitons and the e-h distance of S_1 and S_2 compared to S_3, S_4 and S_5.

Further investigation of these transitions using the contributions of the molecular orbitals in the polymer chain to the e-h shows that both the hole and the electron are distributed between one to two monomers in the case of S_1 and S_2. In contrast, for higher transitions (S_3, S_4, and S_5), the excitons spread out and delocalize over several monomers. As an example, Figure 8 shows the distribution of the hole and the electron for the lowest five singlet excited states of chain number one, which exhibits a typical e-h distribution for a chain in the bulk PDPPTT-T-10 conjugated polymer. The e-h distribution mainly comes from the DPP moiety with some contributions from the TT and T segments (Figure 9). Similar

https://doi.org/10.1021/acs.jpcc.2c01650
J. Phys. Chem. C XXXX, XXX, XXX−XXX

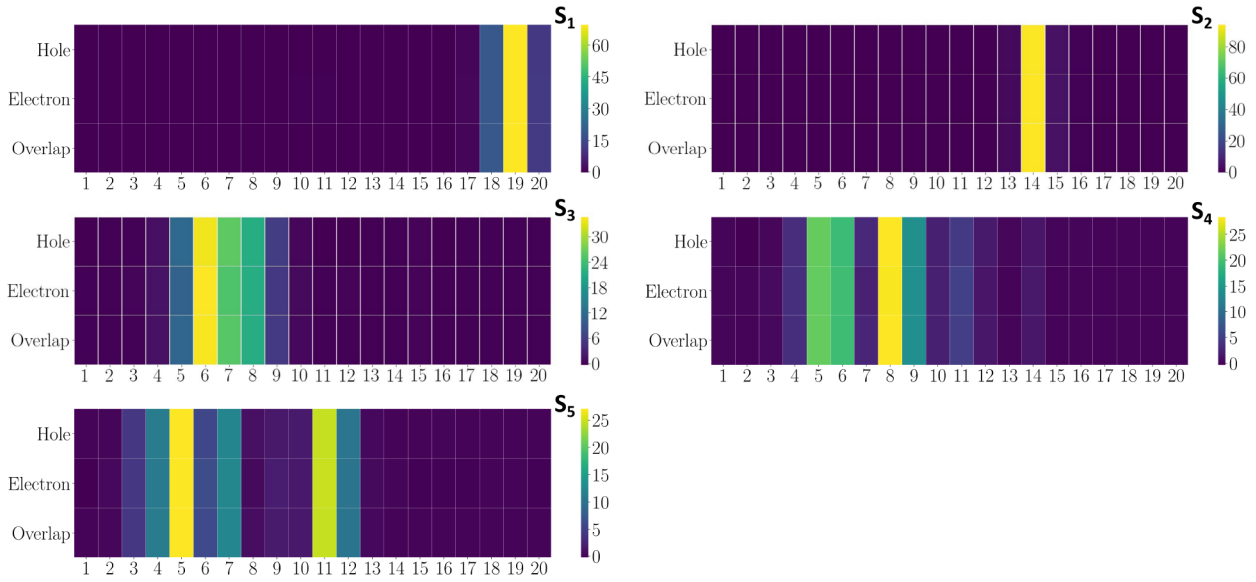

Figure 8. Heat map of the monomer contributions (as a percentage) to the hole and electron for the lowest five excited states of chain number one.

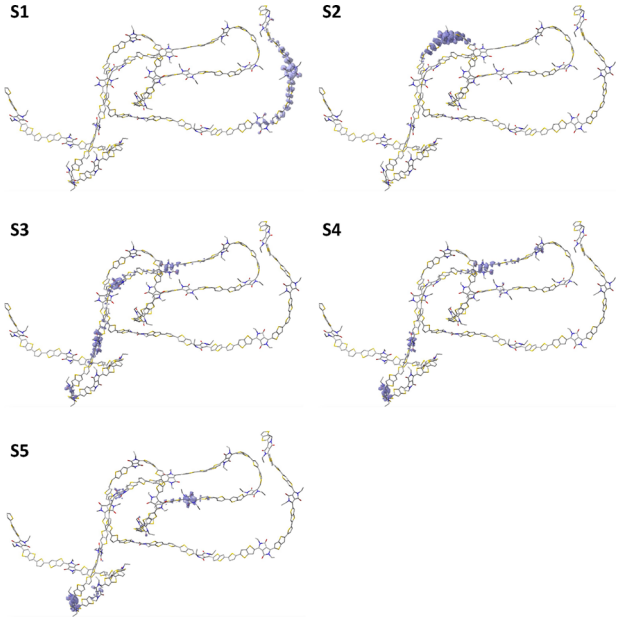

Figure 9. Hole distribution of S_1, S_2, S_3, S_4, and S_5 along chain number one.

trends are also observed for other chains (e.g., Figures S1 and S2). The difference in the extent of the delocalization of the lowest five singlet excitations for PDPPTT-T-10 reveals that one-electron states at the band edge are usually more localized.

Relationships between Chain Conformation and Electronic Structure Properties. Figure 10 shows the folding parameter, nonplanarity parameter, and the contribution of each monomer to the lowest five singlet excited states for chain number one in the 20ch_20mers system. Similar trends are also observed for other chains. Our main goal here is to establish the relationship between the geometric disorder of the polymer chain and its electronic structure properties. It is not straightforward to find any direct correlations from the correspondence in Figure 10a–c. Nevertheless, we can extract some insights. For example, the lower-energy orbitals (i.e., S_1 and S_2) are localized in the region of the chain that is locally

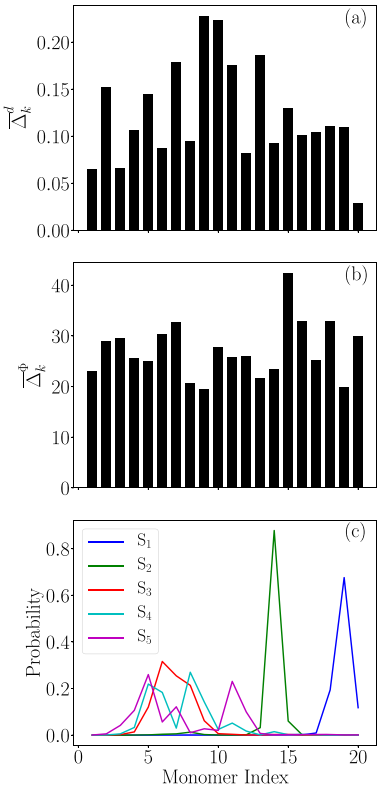

Figure 10. Folding (a) and nonplanarity (b) parameters together with the weight of the transition density on each monomer (c) for chain number one of the 20ch_20mers system.

less folded and more planar (monomers 14 and 19). On the other hand, higher excitations such as S_3, S_4, and S_5 are more delocalized and have the tendency to spread over defects. For instance, there is a significant folding around monomer 9 in chain one (Figure 10a), but S_3, S_4, and S_5 cross this defect. This observation verified that it is challenging to define chromophores in amorphous polymers purely based on the concept of geometric conjugation breaks.[61] An illustration of the distribution of the transition densities of the lowest five

https://doi.org/10.1021/acs.jpcc.2c01650
J. Phys. Chem. C XXXX, XXX, XXX−XXX

excited states along chain one is shown in Figure 11. In general, we find that the lowest excitations (S_1 and S_2) are

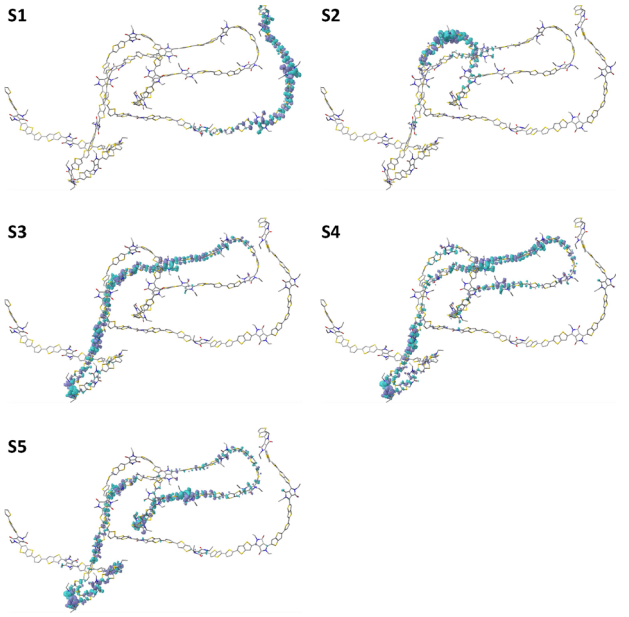

Figure 11. Distribution of transition densities of S_1, S_2, S_3, S_4, and S_5 along chain number one.

typically localized without much overlaps with each other (e.g., see Figures 9 and 11). These excitons are often termed local exciton ground states (LEGSs) derived from empirical model calculations.[62,63] They are considered chromophores for absorption in low-energy windows, and their existence was confirmed for MEH-PPV[37] from first principle calculations. Here, our results for PDPPTT-T-10 further support the presence of LEGSs in amorphous conjugated polymers. Thus, the ability to describe them rigorously from quantum chemical calculations will help construct a reliable exciton transport model for organic semiconducting polymers.

We have revealed the challenge in building a direct relationship between the geometric distortion and the electronic properties of amorphous conjugated polymers. However, we have discovered two interesting things: (i) low-energy excitons tend to avoid disorder and (ii) high-energy excitons may spread over defects. To confirm the preliminary observation more quantitatively, we define several further parameters. First, we introduce $\lambda_f^{\text{chain}} = \sum_{k=1}^{M} \bar{\Delta}_k^{\text{d}}/M$ and $\lambda_p^{\text{chain}} = \sum_{k=1}^{M} \bar{\Delta}_k^{\Phi}/M$, which are essentially the folding and nonplanarity parameters averaged over the whole chain. Next, to obtain the correlation between these order parameters and excited state properties, we compute $\lambda_f^{S_0 \to S_n} = \sum_{k=1}^{M} \bar{\Delta}_k^{\text{d}} P_k^{S_0 \to S_n}$ and $\lambda_p^{S_0 \to S_n} = \sum_{k=1}^{M} \bar{\Delta}_k^{\Phi} P_k^{S_0 \to S_n}$, which are the average folding and nonplanarity parameters weighted by the $S_0 \to S_n$ transition density $P_k^{S_0 \to S_n}$ on each monomer k. These two parameters describe how folded and/or nonplanar a polymer chain is in the region where the transition $S_0 \to S_n$ is located. In addition, we also compute the folding and nonplanarity degree of a chain in the region where the orbital (e.g., HOMO) is localized as $\lambda_f^{\text{HOMO}} = \sum_{k=1}^{M} \Delta_k^{\text{d}} P_k^{\text{HOMO}}$ and $\lambda_p^{\text{HOMO}} = \sum_{k=1}^{M} \bar{\Delta}_k^{\Phi} P_k^{\text{HOMO}}$. Here, P_k^{HOMO} is the HOMO orbital density on monomer k.

By comparing the distribution of these parameters, we can establish the correlation between the order parameters and the position of the excitons. Figure 12 shows the histogram

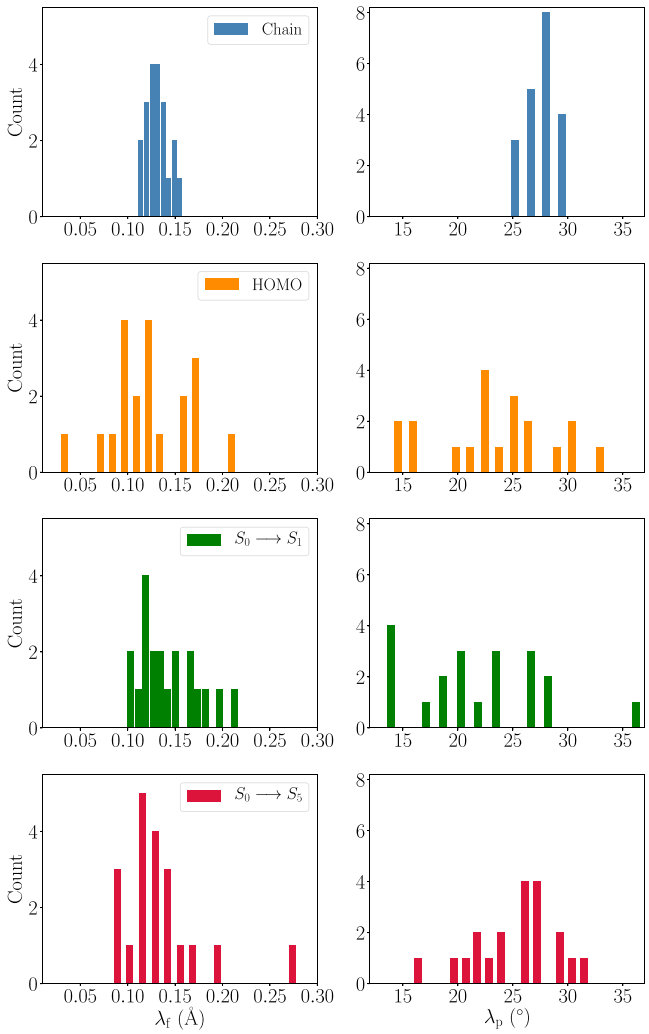

Figure 12. Distributions of chain folding (left panels) and nonplanarity (right panels) of the 20ch_20mers system. Blue bars are the distribution of the average chain folding (λ_f^{chain}) and nonplanarity (λ_p^{chain}) per chain. Orange bars are the distribution of the HOMO (per monomer) weighted average chain folding (λ_f^{HOMO}) and nonplanarity (λ_p^{HOMO}). Green bars are the distribution of the $S_0 \to S_1$ transition density ($P_k^{S_0 \to S_1}$) weighted average chain folding ($\lambda_f^{S_0 \to S_1}$) and nonplanarity ($\lambda_p^{S_0 \to S_1}$). Red bars are the distribution of the $S_0 \to S_5$ transition density ($P_k^{S_0 \to S_5}$) weighted average chain folding ($\lambda_f^{S_0 \to S_5}$) and nonplanarity ($\lambda_p^{S_0 \to S_5}$).

distribution of the folding (λ_f) and the nonplanarity (λ_p) for the chain (blue), HOMO (orange), $S_0 \to S_1$ transition (green), and $S_0 \to S_5$ transition (red) for the 20ch_20mers system. For clarity, we exclude data for other orbitals and transitions. Figure 12 shows that the order parameters (λ_f and λ_p) in the region of the HOMO have a similar distribution to those where the $S_0 \to S_1$ and $S_0 \to S_5$ transitions are distributed. This implied that the HOMO has a significant contribution to these transitions. Generally, if orbitals and/or the exciton try to avoid defects in the polymer chains, we will not observe any overlap between the distribution of the chain defects and others (e.g., between λ_p^{chain} and λ_p^{HOMO}). However, we can see that it is not the case here. For example, Figure 12b shows that λ_p^{chain} is distributed in the range [25°, 30°] with a peak at about 28°, while $\lambda_p^{S_0 \to S_1}$ varies in a broad range between 13 and 37°. This means that although the $S_0 \to S_1$ transition (also the HOMO) tends to stay away from the nonplanar region of the chain, they

https://doi.org/10.1021/acs.jpcc.2c01650
J. Phys. Chem. C XXXX, XXX, XXX−XXX

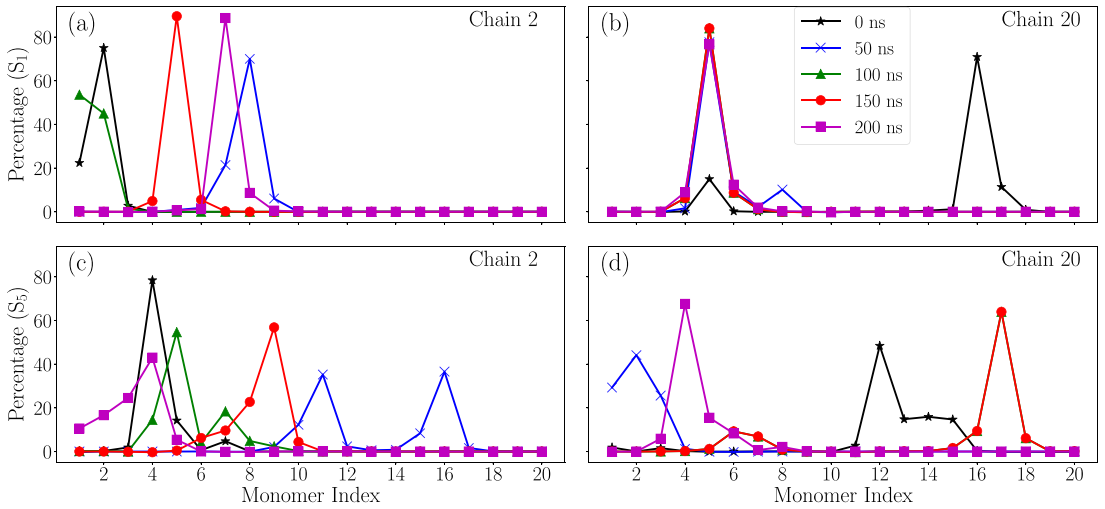

Figure 13. Exciton evolution along polymer chains at 0 (star black line), 50 (cross blue line), 100 (triangle green line), 150 (circle red line), and 200 ns (square magenta line). (a) S_1 hole of chain 2, (b) S_1 hole of chain 20, (c) S_5 hole of chain 2, and S_5 hole of chain 20.

are often found spreading over defects. On the other hand, distribution of the nonplanarity of the $S_0 \rightarrow S_5$ transition overlaps quite well with λ_p^{chain}, indicating a more delocalized character over nonplanar regions of the higher excited states.

A similar observation can also be made for the case of the folding parameters (Figure 12a). Although both HOMO and excitons try to stay away from the chain defects, they are also often found at the average folding locations of the chain. It was suggested that defects (folding and nonplanarity) break the polymer chain into fragments in which excitons are localized.[61] However, our results confirm that pure geometric definition of a chromophore or exciton is not advisable for amorphous polymers. Definitions based on the electron density are crucial, and explicit quantum chemical calculations should be carried out before formulating exciton transport models.

Having confirmed that the inter-chain excitonic couplings are negligible, we focus on analyzing the evolution of the exciton along the polymer chains. More specifically, we investigate the hole dynamics for different transitions on different chains. Figure 13 shows the monomer contributions to $S_0 \rightarrow S_1$ and $S_0 \rightarrow S_5$ transitions for two representative chains (2 and 20) of the 20ch_20mers system at different times. The nuclear trajectories are taken from a 200 ns equilibrium run, separated by 50 ns. Since the polymer is in its amorphous state under the studied conditions, the overall chain conformation does not change significantly over tens of nanoseconds. However, this is certainly not the case for the excited state properties for which the timescale is much shorter.

Figure 13 shows that excitons of both $S_0 \rightarrow S_1$ and $S_0 \rightarrow S_5$ transitions can move freely back and forth along the polymer chains. The centroid positions of excitons change considerably with time. While the shape of the lowest excited state ($S_0 \rightarrow S_1$) remains almost unchanged, that of the higher transition ($S_0 \rightarrow S_5$) varies significantly with time. The modulation of the exciton's size and shape is partly due to the fluctuation of the torsion angles, which effectively manipulates the magnitude of the intra-chain excitonic couplings. In addition, we also observe a variation of the orbital localization lengths (Figure S4), which is the result of the change in the shape of the DOS and the interchange of different molecular orbitals due to the evolution of the polymer chains. Thus, the conformational rearrangement of the polymer chain over time may alter the location, shape, and energetic order of excited states but tends not to affect the nature of the low energy excitons (i.e., LEGS). Another critical point to note here is that the dynamics of the nuclei are much slower than that of the excitons; analysis based on a couple of snapshots is still sufficient to give a reliable picture of the excited states in amorphous polymers. Our results here for PDPPTT-T-10 are very similar to what was observed for MEH-PPV,[36,37] which suggest these properties could be standard features for amorphous conjugated polymers.

CONCLUSIONS AND OUTLOOK

This paper employs a range of computational tools to characterize the relationships between the morphology and electronic structure properties of amorphous conjugated PDPPTT-T-10 polymers. First of all, the force field parameters for these systems are carefully optimized to ensure that the classical potential energy surface and its gradients of the polymer are mapped onto the targeted ab initio ones. Then, MD simulation is utilized to generate amorphous polymer models, and the equilibrium trajectories are sampled. After that, large-scale TDDFT calculations for the electronic excited states of the polymeric systems are performed to obtain the structure−property relationships. Given the size of the polymeric system, a balanced set of approximations is determined to provide the most accurate excited state calculations for the bulk PDPPTT-T-10 polymer models.

Our calculations reveal that the effects of the side-chain on the electronic structure properties of the polymer chain are minor, especially near the band edge. The electronic structure is chiefly determined by the conformational disorder of the chain backbone. Our polymer models are large enough to reproduce the electronic structure properties, such as the density of states and the localization length, of the bulk system. We also confirm that the electronic couplings between polymer chains are negligibly small (mostly less than 5 meV), and the effect of electrostatic disorder is insignificant. This suggests that the exciton transport mechanism along the chain could be described by incoherent hopping. We observe that the excitons of PDPPTT-T-10 prefer to localize in regions that are relatively planar and less folded. However, exceptions are not

https://doi.org/10.1021/acs.jpcc.2c01650
J. Phys. Chem. C XXXX, XXX, XXX−XXX

rare, and these excitons can spread over defects. Thus, it is not possible to define a chromophore in this polymer purely based on geometric conjugation breaks. A rigorous definition can only be made based on evaluating the polymer excited state wave function. Hence, our results provide useful information for constructing more realistic models for the exciton dynamics study of this class of polymeric materials.

■ ASSOCIATED CONTENT

Supporting Information

The Supporting Information is available free of charge at https://pubs.acs.org/doi/10.1021/acs.jpcc.2c01650.

Force field development procedure and MD simulation details; definition of P_k^m and $P_k^{S_0 \rightarrow S_n}$; and additional properties of the polymer (PDF)

Force field parameters, input files for various calculations, and related analysis scripts (ZIP)

■ AUTHOR INFORMATION

Corresponding Authors

Jonathan D. Hirst − *School of Chemistry, University of Nottingham, Nottingham NG7 2RD, U.K.;* orcid.org/0000-0002-2726-0983; Email: jonathan.hirst@nottingham.ac.uk

Hainam Do − *Department of Chemical and Environmental Engineering and Key Laboratory of Carbonaceous Waste Processing and Process Intensification Research of Zhejiang Province, University of Nottingham Ningbo China, Ningbo 315100, China; New Materials Institute, University of Nottingham Ningbo China, Ningbo 315042, China;* orcid.org/0000-0003-4239-6157; Email: hainam.do@nottingham.edu.cn

Author

Ling Jiang − *Department of Chemical and Environmental Engineering, University of Nottingham Ningbo China, Ningbo 315100, China*

Complete contact information is available at: https://pubs.acs.org/10.1021/acs.jpcc.2c01650

Notes

The authors declare no competing financial interest.

■ ACKNOWLEDGMENTS

We are grateful for access to the University of Nottingham High Performance Computing Facility both in Ningbo China and Nottingham UK. L.J. thanks the Faculty of Science and Engineering at University of Nottingham Ningbo China for a PhD scholarship. H.D. is supported by The Research Fund for International Young Scientists (grant no. 21850410456). This work is financially supported by the Natural Science Foundation of China (grant nos. 21875106 and 22171153). J.D.H. is supported by the Royal Academy of Engineering under the Chairs in Emerging Technologies scheme. The Zhejiang Provincial Department of Science and Technology is acknowledged for this research under its Provincial Key Laboratory Programme (2020E10018).

■ DEDICATION

Dedicated to the memory to our dear friend and colleague, Professor Nick Besley.

■ REFERENCES

(1) Kippelen, B.; Brédas, J.-L. Organic photovoltaics. *Energy Environ. Sci.* **2009**, *2*, 251−261.

(2) Lin, Y.; Zhao, F.; He, Q.; Huo, L.; Wu, Y.; Parker, T. C.; Ma, W.; Sun, Y.; Wang, C.; Zhu, D.; et al. High-performance electron acceptor with thienyl side chains for organic photovoltaics. *J. Am. Chem. Soc.* **2016**, *138*, 4955−4961.

(3) Li, Y.; Guo, X.; Peng, Z.; Qu, B.; Yan, H.; Ade, H.; Zhang, M.; Forrest, S. R. Color-neutral, semitransparent organic photovoltaics for power window applications. *Proc. Natl. Acad. Sci. U. S. A.* **2020**, *117*, 21147−21154.

(4) Li, Y.; Huang, X.; Ding, K.; Sheriff, H. K.; Ye, L.; Liu, H.; Li, C.-Z.; Ade, H.; Forrest, S. R. Non-fullerene acceptor organic photovoltaics with intrinsic operational lifetimes over 30 years. *Nat. Commun.* **2021**, *12*, 1−9.

(5) Schön, J. H.; Meng, H.; Bao, Z. Self-assembled monolayer organic field-effect transistors. *Nature* **2001**, *413*, 713−716.

(6) Muccini, M. A bright future for organic field-effect transistors. *Nat. Mater.* **2006**, *5*, 605−613.

(7) Matsushima, T.; Bencheikh, F.; Komino, T.; Leyden, M. R.; Sandanayaka, A. S.; Qin, C.; Adachi, C. High performance from extraordinarily thick organic light-emitting diodes. *Nature* **2019**, *572*, 502−506.

(8) Zou, S.-J.; Shen, Y.; Xie, F.-M.; Chen, J.-D.; Li, Y.-Q.; Tang, J.-X. Recent advances in organic light-emitting diodes: toward smart lighting and displays. *Mater. Chem. Front.* **2020**, *4*, 788−820.

(9) Inal, S.; Rivnay, J.; Suiu, A.-O.; Malliaras, G. G.; McCulloch, I. Conjugated polymers in bioelectronics. *Acc. Chem. Res.* **2018**, *51*, 1368−1376.

(10) Sekitani, T. A photocurable bioelectronics−tissue interface. *Nat. Mater.* **2021**, *20*, 1460−1461.

(11) Fratini, S.; Nikolka, M.; Salleo, A.; Schweicher, G.; Sirringhaus, H. Charge transport in high-mobility conjugated polymers and molecular semiconductors. *Nat. Mater.* **2020**, *19*, 491−502.

(12) Zhu, J.; Zhang, Z.; Lv, Y.; Lan, A.; Lu, H.; Do, H.; Chen, F. Organic solar cells based on non-fullerene acceptors containing thiophene [3, 2-b] pyrrole. *Org. Electron.* **2022**, *103*, 106461.

(13) Brédas, J.-L.; Calbert, J. P.; da Silva Filho, D.; Cornil, J. Organic semiconductors: A theoretical characterization of the basic parameters governing charge transport. *Proc. Natl. Acad. Sci. U. S. A.* **2002**, *99*, 5804−5809.

(14) Xu, Y.; Sun, H.; Li, W.; Lin, Y.-F.; Balestra, F.; Ghibaudo, G.; Noh, Y.-Y. Exploring the charge transport in conjugated polymers. *Adv. Mater.* **2017**, *29*, 1702729.

(15) McCulloch, I.; Heeney, M.; Bailey, C.; Genevicius, K.; MacDonald, I.; Shkunov, M.; Sparrowe, D.; Tierney, S.; Wagner, R.; Zhang, W.; et al. Liquid-crystalline semiconducting polymers with high charge-carrier mobility. *Nat. Mater.* **2006**, *5*, 328−333.

(16) Wang, Y.; Sun, L.; Wang, C.; Yang, F.; Ren, X.; Zhang, X.; Dong, H.; Hu, W. Organic crystalline materials in flexible electronics. *Chem. Soc. Rev.* **2019**, *48*, 1492−1530.

(17) Ong, B. S.; Wu, Y.; Liu, P.; Gardner, S. High-performance semiconducting polythiophenes for organic thin-film transistors. *J. Am. Chem. Soc.* **2004**, *126*, 3378−3379.

(18) DeLongchamp, D. M.; Kline, R. J.; Lin, E. K.; Fischer, D. A.; Richter, L. J.; Lucas, L. A.; Heeney, M.; McCulloch, I.; Northrup, J. E. High carrier mobility polythiophene thin films: structure determination by experiment and theory. *Adv. Mater.* **2007**, *19*, 833−837.

(19) Nielsen, C. B.; Turbiez, M.; McCulloch, I. Recent advances in the development of semiconducting DPP-containing polymers for transistor applications. *Adv. Mater.* **2013**, *25*, 1859−1880.

(20) Venkateshvaran, D.; Nikolka, M.; Sadhanala, A.; Lemaur, V.; Zelazny, M.; Kepa, M.; Hurhangee, M.; Kronemeijer, A. J.; Pecunia, V.; Nasrallah, I.; et al. Approaching disorder-free transport in high-mobility conjugated polymers. *Nature* **2014**, *515*, 384−388.

(21) DuBay, K. H.; Hall, M. L.; Hughes, T. F.; Wu, C.; Reichman, D. R.; Friesner, R. A. Accurate force field development for modeling conjugated polymers. *J. Chem. Theory Comput.* **2012**, *8*, 4556−4569.

https://doi.org/10.1021/acs.jpcc.2c01650
J. Phys. Chem. C XXXX, XXX, XXX−XXX

(22) Gartner, T. E., III; Jayaraman, A. Modeling and simulations of polymers: a roadmap. *Macromolecules* **2019**, *52*, 755−786.
(23) Wessels, M. G.; Jayaraman, A. Molecular dynamics simulation study of linear, bottle-brush, and star-like amphiphilic block polymer assembly in solution. *Soft Matter* **2019**, *15*, 3987−3998.
(24) Jiang, L.; Rogers, D. M.; Hirst, J. D.; Do, H. Force fields for macromolecular assemblies containing diketopyrrolopyrrole and thiophene. *J. Chem. Theory Comput.* **2020**, *16*, 5150−5162.
(25) Nayyar, I. H.; Batista, E. R.; Tretiak, S.; Saxena, A.; Smith, D. L.; Martin, R. L. Role of geometric distortion and polarization in localizing electronic excitations in conjugated polymers. *J. Chem. Theory Comput.* **2013**, *9*, 1144−1154.
(26) Panda, A. N.; Plasser, F.; Aquino, A. J.; Burghardt, I.; Lischka, H. Electronically excited states in poly (p-phenylenevinylene): vertical excitations and torsional potentials from high-level ab initio calculations. *J. Phys. Chem. A* **2013**, *117*, 2181−2189.
(27) Roseli, R. B.; Tapping, P. C.; Kee, T. W. Origin of the excited-state absorption spectrum of polythiophene. *J. Phys. Chem. Lett.* **2017**, *8*, 2806−2811.
(28) Matta, M.; Pezzella, A.; Troisi, A. Relation between local structure, electric dipole, and charge carrier dynamics in DHICA melanin: a model for biocompatible semiconductors. *J. Phys. Chem. Lett.* **2020**, *11*, 1045−1051.
(29) Simine, L.; Rossky, P. J. Relating chromophoric and structural disorder in conjugated polymers. *J. Phys. Chem. Lett.* **2017**, *8*, 1752−1756.
(30) Liu, T.; Troisi, A. Understanding the microscopic origin of the very high charge mobility in PBTTT: tolerance of thermal disorder. *Adv. Funct. Mater.* **2014**, *24*, 925−933.
(31) Cheung, D.; McMahon, D. P.; Troisi, A. A realistic description of the charge carrier wave function in microcrystalline polymer semiconductors. *J. Am. Chem. Soc.* **2009**, *131*, 11179−11186.
(32) Cheung, D. L.; McMahon, D. P.; Troisi, A. Computational study of the structure and charge-transfer parameters in low-molecular-mass P3HT. *J. Phys. Chem. B* **2009**, *113*, 9393−9401.
(33) Granadino-Roldán, J.; Vukmirović, N.; Fernández-Gómez, M.; Wang, L.-W. The role of disorder on the electronic structure of conjugated polymers. The case of poly-2, 5-bis (phenylethynyl)-1, 3, 4-thiadiazole. *Phys. Chem. Chem. Phys.* **2011**, *13*, 14500−14509.
(34) Vukmirovic, N.; Wang, L.-W. Density of states and wave function localization in disordered conjugated polymers: a large scale computational study. *J. Phys. Chem. B* **2011**, *115*, 1792−1797.
(35) Poelking, C.; Cho, E.; Malafeev, A.; Ivanov, V.; Kremer, K.; Risko, C.; Brédas, J.-L.; Andrienko, D. Characterization of charge-carrier transport in semicrystalline polymers: electronic couplings, site energies, and charge-carrier dynamics in poly (bithiophene-alt-thienothiophene)[PBTTT]. *J. Phys. Chem. C* **2013**, *117*, 1633−1640.
(36) Qin, T.; Troisi, A. Relation between structure and electronic properties of amorphous MEH-PPV polymers. *J. Am. Chem. Soc.* **2013**, *135*, 11247−11256.
(37) Ma, H.; Qin, T.; Troisi, A. Electronic excited states in amorphous MEH-PPV polymers from large-scale first principles calculations. *J. Chem. Theory Comput.* **2014**, *10*, 1272−1282.
(38) Wienk, M. M.; Turbiez, M.; Gilot, J.; Janssen, R. A. Narrow-bandgap diketo-pyrrolopyrrole polymer solar cells: the effect of processing on the performance. *Adv. Mater.* **2008**, *20*, 2556−2560.
(39) Bijleveld, J. C.; Zoombelt, A. P.; Mathijssen, S. G.; Wienk, M. M.; Turbiez, M.; de Leeuw, D. M.; Janssen, R. A. Poly (diketopyrrolopyrrole- terthiophene) for Ambipolar Logic and Photovoltaics. *J. Am. Chem. Soc.* **2009**, *131*, 16616−16617.
(40) Ashraf, R. S.; Chen, Z.; Leem, D. S.; Bronstein, H.; Zhang, W.; Schroeder, B.; Geerts, Y.; Smith, J.; Watkins, S.; Anthopoulos, T. D.; et al. Silaindacenodithiophene semiconducting polymers for efficient solar cells and high-mobility ambipolar transistors. *Chem. Mater.* **2011**, *23*, 768−770.
(41) Shin, J.; Park, G. E.; Lee, D. H.; Um, H. A.; Lee, T. W.; Cho, M. J.; Choi, D. H. Bis (thienothiophenyl) diketopyrrolopyrrole-based conjugated polymers with various branched alkyl side chains and their applications in thin-film transistors and polymer solar cells. *ACS Appl. Mater. Interfaces* **2015**, *7*, 3280−3288.
(42) Nelson, T. L.; Young, T. M.; Liu, J.; Mishra, S. P.; Belot, J. A.; Balliet, C. L.; Javier, A. E.; Kowalewski, T.; McCullough, R. D. Transistor paint: high mobilities in small bandgap polymer semiconductor based on the strong acceptor, diketopyrrolopyrrole and strong donor, dithienopyrrole. *Adv. Mater.* **2010**, *22*, 4617−4621.
(43) Bronstein, H.; Chen, Z.; Ashraf, R. S.; Zhang, W.; Du, J.; Durrant, J. R.; Shakya Tuladhar, P.; Song, K.; Watkins, S. E.; Geerts, Y.; et al. Thieno [3, 2-b] thiophene-diketopyrrolopyrrole-containing polymers for high-performance organic field-effect transistors and organic photovoltaic devices. *J. Am. Chem. Soc.* **2011**, *133*, 3272−3275.
(44) Noriega, R.; Rivnay, J.; Vandewal, K.; Koch, F. P.; Stingelin, N.; Smith, P.; Toney, M. F.; Salleo, A. A general relationship between disorder, aggregation and charge transport in conjugated polymers. *Nat. Mater.* **2013**, *12*, 1038−1044.
(45) Do, H.; Troisi, A. Developing accurate molecular mechanics force fields for conjugated molecular systems. *Phys. Chem. Chem. Phys.* **2015**, *17*, 25123−25132.
(46) Phillips, J. C.; Braun, R.; Wang, W.; Gumbart, J.; Tajkhorshid, E.; Villa, E.; Chipot, C.; Skeel, R. D.; Kalé, L.; Schulten, K. Scalable molecular dynamics with NAMD. *J. Comput. Chem.* **2005**, *26*, 1781−1802.
(47) Siepmann, J. I.; Frenkel, D. Configurational bias Monte Carlo: a new sampling scheme for flexible chains. *Mol. Phys.* **1992**, *75*, 59−70.
(48) Callaway, C. P.; Bombile, J. H.; Mask, W.; Ryno, S. M.; Risko, C. Thermomechanical enhancement of DPP-4T through purposeful π-conjugation disruption. *J. Polym. Sci.* **2022**, *60*, 559−568.
(49) Reisjalali, M.; Burgos-Mármol, J. J.; Manurung, R.; Troisi, A. Local structuring of diketopyrrolopyrrole (DPP)-based oligomers from molecular dynamics simulations. *Phys. Chem. Chem. Phys.* **2021**, *23*, 19693−19707.
(50) Chai, J.-D.; Head-Gordon, M. Long-range corrected hybrid density functionals with damped atom−atom dispersion corrections. *Phys. Chem. Chem. Phys.* **2008**, *10*, 6615−6620.
(51) Hertwig, R. H.; Koch, W. On the parameterization of the local correlation functional. What is Becke-3-LYP? *Chem. Phys. Lett.* **1997**, *268*, 345−351.
(52) Yanai, T.; Tew, D. P.; Handy, N. C. A new hybrid exchange−correlation functional using the Coulomb-attenuating method (CAM-B3LYP). *Chem. Phys. Lett.* **2004**, *393*, 51−57.
(53) Zhao, Y.; Truhlar, D. G. Density functional calculations of E2 and SN2 reactions: effects of the choice of density functional, basis set, and self-consistent iterations. *J. Chem. Theory Comput.* **2010**, *6*, 1104−1108.
(54) Frisch, M. J. et al.*Gaussian 16*, Revision C.01. Gaussian, Inc.: Wallingford, CT, 2016.
(55) Lu, T.; Chen, F. Multiwfn: a multifunctional wavefunction analyzer. *J. Comput. Chem.* **2012**, *33*, 580−592.
(56) Liu, Z.; Lu, T.; Chen, Q. An sp-hybridized all-carboatomic ring, cyclo [18] carbon: Electronic structure, electronic spectrum, and optical nonlinearity. *Carbon* **2020**, *165*, 461−467.
(57) Guido, C. A.; Cortona, P.; Mennucci, B.; Adamo, C. On the metric of charge transfer molecular excitations: a simple chemical descriptor. *J. Chem. Theory Comput.* **2013**, *9*, 3118−3126.
(58) Adamo, C.; Jacquemin, D. The calculations of excited-state properties with Time-Dependent Density Functional Theory. *Chem. Soc. Rev.* **2013**, *42*, 845−856.
(59) Tawada, Y.; Tsuneda, T.; Yanagisawa, S.; Yanai, T.; Hirao, K. A long-range-corrected time-dependent density functional theory. *J. Chem. Phys.* **2004**, *120*, 8425−8433.
(60) Dreuw, A.; Weisman, J. L.; Head-Gordon, M. Long-range charge-transfer excited states in time-dependent density functional theory require non-local exchange. *J. Chem. Phys.* **2003**, *119*, 2943−2946.
(61) Collini, E.; Scholes, G. D. Coherent intrachain energy migration in a conjugated polymer at room temperature. *Science* **2009**, *323*, 369−373.

https://doi.org/10.1021/acs.jpcc.2c01650
J. Phys. Chem. C XXXX, XXX, XXX−XXX

(62) Makhov, D. V.; Barford, W. Local exciton ground states in disordered polymers. *Phys. Rev. B* **2010**, *81*, 165201.
(63) Barford, W.; Mannouch, J. R. Torsionally induced exciton localization and decoherence in π-conjugated polymers. *J. Chem. Phys.* **2018**, *149*, 214107.

https://doi.org/10.1021/acs.jpcc.2c01650
J. Phys. Chem. C XXXX, XXX, XXX−XXX